Supplementary Information

Thermally induced carbonation of $Ca(OH)_2$ in CO_2 atmosphere: Kinetic simulation of overlapping mass-loss and mass-gain processes in solid–gas system

Nobuyoshi Koga* and Satoki Kodani
Department of Science Education, Graduate School of Education, Hiroshima University, 1-1-1 Kagamiyama, Higashi-Hiroshima 739-8524, Japan

Contents

S1. Calibration of TG–DTA instruments s1

S2. Sample characterization s2

S3. Thermal behavior of $Ca(OH)_2$ in an inert gas atmosphere s2

S4. Kinetics of the thermal decomposition of $Ca(OH)_2$ s3

S5. Thermal behavior of $Ca(OH)_2$ in CO_2 atmosphere s5

S6. Kinetics of the thermally induced carbonation of $Ca(OH)_2$ s6

S1. Calibration of TG–DTA instruments

All the TG–DTA instruments (TG/DTA220, TG-8120, and Thermoplus Evo2) used in this study are characterized by a horizontally arranged differential balance and two balance beams symmetrically arranged in furnaces are composed of R-type thermocouple. These instruments were preliminarily calibrated in relation to the mass change and temperature. The calibration with respect to the change in mass value was performed at room temperature by the addition/removal of a 10-mg standard weight to/from the sample holder. Subsequently, the accuracy of the mass-change values at high temperatures was confirmed by measuring the mass change associated with the thermal decomposition of a sample of calcium oxalate monohydrate (>99.9985%, Alfa Acer) under measurement conditions identical to those used for the study sample. The temperature calibration of the TG–DTA instruments (TG/DTA220, Thermoplus Evo2, and TG-8120) was carried out in reference to the melting points of pure metals (In, Sn, Pb, Zn, Al, and Ag, >99.99%, Nilaco) by determining the onset temperature of the endothermic DTA peak. For the TG–DTA measurements using TG/DTA220 and Thermoplus Evo2, approximately 5.0 mg of Al_2O_3 (>99.99%) weighed into a platinum pan, which is paired with that for the sample, were used as the reference material for the DTA and as the counter balance of the differential balance system. An empty platinum pan was used as the reference and counter balance for the TG/DTA–MS measurements using TG-8120 to avoid any possible contamination of the evolved gas. All TG–DTA curves were subjected to baseline correction prior to data analysis using blank data recorded under conditions identical to those used for the sample measurements.

* Corresponding Author. Tel/Fax: +81-82-424-7092; e-mail: nkoga@hiroshima-u.ac.jp

S2. Sample characterization

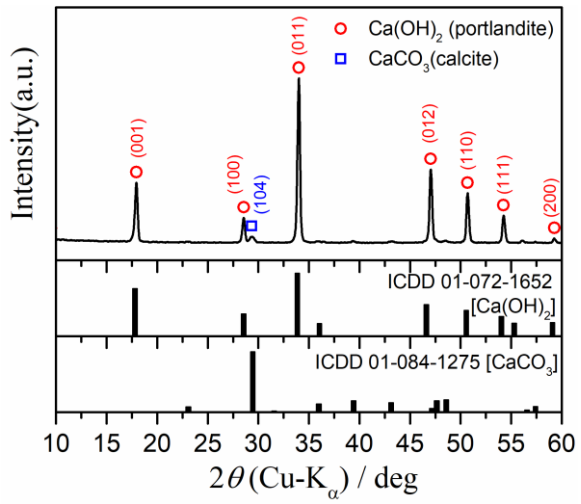

Figure S1. XRD pattern of the $Ca(OH)_2$ sample.

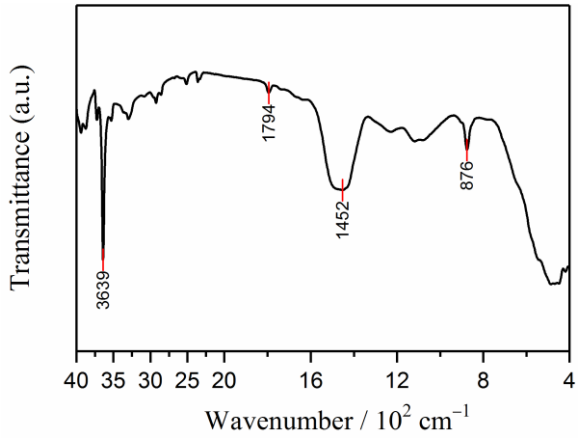

Figure S2. FT-IR spectrum of the $Ca(OH)_2$ sample.

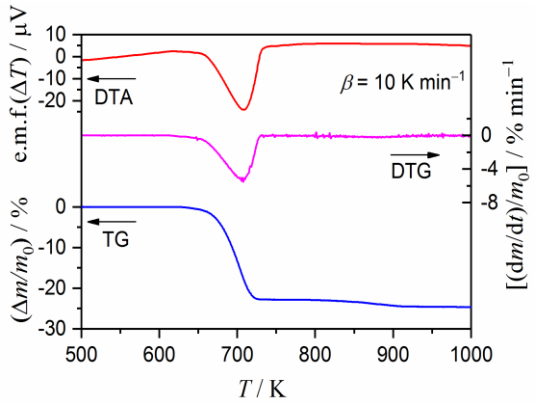

Figure S3. TG–DTG–DTA curves of $Ca(OH)_2$ sample (approximately 10 mg) recorded at $\beta = 10$ K min^{-1} in a stream of N_2 gas (flow rate: 300 cm^3 min^{-1}).

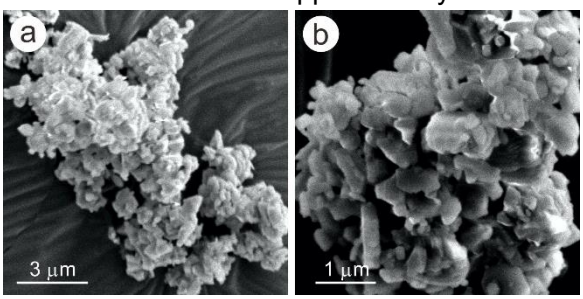

Figure S4. SEM images of the $Ca(OH)_2$ sample: (a) ×5,000 and (b) ×10,000 magnification.

S3. Thermal behavior of $Ca(OH)_2$ in an inert gas atmosphere

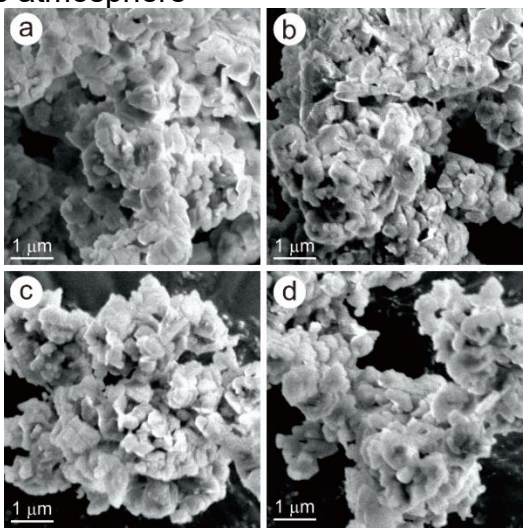

Figure S5. Typical SEM images of the sample particles that had undergone partial decomposition as a consequence of being heated linearly to different final temperatures at $\beta = 5$ K min^{-1} in a stream of N_2 gas (flow rate: 300 cm^3 min^{-1}): (a) $T = 623$ K ($\alpha = 0.00$), (b) $T = 673$ K ($\alpha = 0.13$), (c) $T = 698$ K ($\alpha = 0.54$), and (d) $T = 973$ K ($\alpha = 1.00$).

S4. Kinetics of the thermal decomposition of $Ca(OH)_2$

(1) Kinetic data

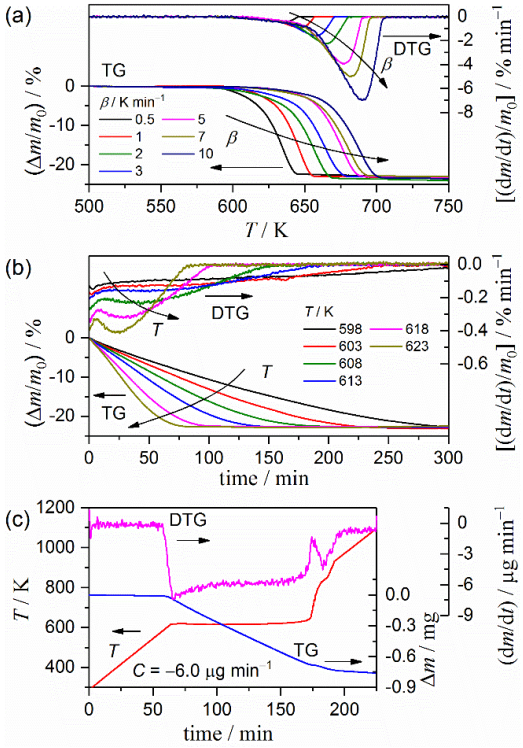

Figure S6. TG–DTG curves for the thermal decomposition of $Ca(OH)_2$ (m_0 = 3.00 ± 0.05 mg) recorded as the reaction was conducted in a stream of N_2 gas (flow rate: 300 cm^3 min^{-1}) under (a) liner nonisothermal conditions at different β, (b) isothermal conditions at different constant T, and (c) controlled transformation rate conditions at $C = -6.0$ μg min^{-1}.

(2) Mathematical deconvolution and subsequent formal kinetic analysis

The Weibull function was used as $F(t)$ in eq. (5) for the mathematical deconvolution of DTG curves, because a statistical function to be able to fit asymmetric peaks is generally suitable to the deconvolution of overlapping solid-state reactions.

$$F(t) = a_0\left(\frac{a_3-1}{a_3}\right)^{(1-a_3)/a_3}\left\{\frac{t-a_1}{a_2}+\left(\frac{a_3-1}{a_3}\right)^{1/a_3}\right\}^{a_3-1} \times \exp\left[-\left\{\frac{t-a_1}{a_2}+\left(\frac{a_3-1}{a_3}\right)^{1/a_3}\right\}^{a_3}+\frac{a_3-1}{a_3}\right] \quad \text{(S1)}$$

where a_0-a_3 are the amplitude, center, width, and shape, respectively. In Figure S7 are reported the typical results of the mathematical deconvolution of a DTG curve. From the mathematically separated DTG curves, the contribution c of each reaction step i to the overall reaction can be roughly estimated from the peak areas. In Table S1 are summarized the contributions (c_i) of each reaction step estimated from the DTG curves at different β and those average values. The estimated c_i values were nearly constant irrespective of β, and the average values of (c_1, c_2) were determined to be (0.24 ± 0.01, 0.76 ± 0.01), respectively.

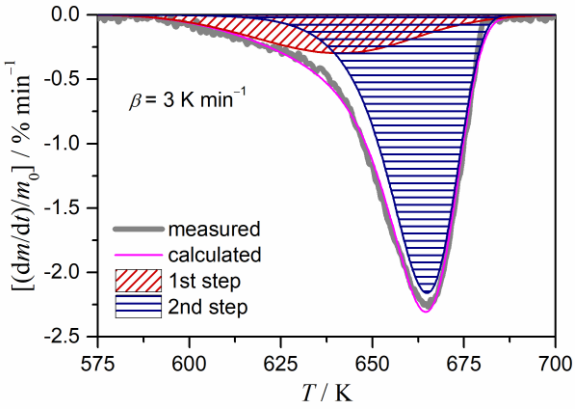

Figure S7. A typical result of the mathematical deconvolution of the DTG curve for the thermal decomposition of $Ca(OH)_2$ recorded at β = 3 K min^{-1} in a stream of N_2 gas.

Table S1. The contributions, c_1 and c_2, of each reaction step of the thermal decomposition of $Ca(OH)_2$ estimated by way of the mathematical deconvolution of the DTG curves recorded at different β

β / K min^{-1}	c_1	c_2
0.5	0.23	0.77
1.0	0.23	0.77
2.0	0.25	0.75
3.0	0.23	0.77
5.0	0.25	0.75
7.0	0.24	0.76
10.0	0.24	0.76
Average	0.24 ± 0.01	0.76 ± 0.01

The individual DTG curves for the first and second reaction steps can be converted to a series of kinetic data (Figure S8). These kinetic data generally indicate a systematic shift to higher temperatures as the value of β increases. The individual sets of kinetic data were assumed to be described as the single step reaction and analyzed by the isoconversional method based on eq. (4). In Figure S9 are summarized the results of the isoconversional kinetic analysis applied to the mathematically separated first and second reaction steps. The plots of $\ln(d\alpha_i/dt)$ versus T^{-1} were characterized by a statistically significant linearity, irrespective of the α_i value, for both reaction steps (Figure S9(a) and (b)). Although the slopes of the plots were practically constant for the second reaction step, a systematic increase in the slope was observed for the first reaction step. Therefore, the apparent $E_{a,1}$ values at different α_1 increased gradually from ~125 kJ mol^{-1} to ~225 kJ mol^{-1}. On the other hand, the apparent $E_{a,2}$ had a practically constant value with the average value of

183.2 ± 0.9 kJ mol^{-1} in the $0.10 \leq \alpha_2 \leq 0.90$ range. The results for the second reaction step is ideal as a single step reaction, but further considerations are required for describing the variation of $E_{a,1}$ as the reaction progresses.

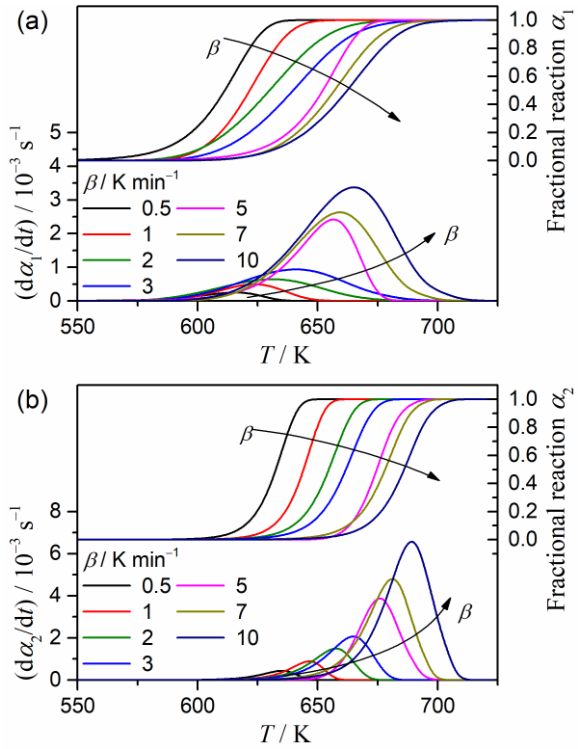

Figure S8. Kinetic curves for each reaction step of the thermal decomposition of $Ca(OH)_2$ obtained by the mathematical deconvolution of DTG curves: (a) the first reaction step and (b) the second reaction step.

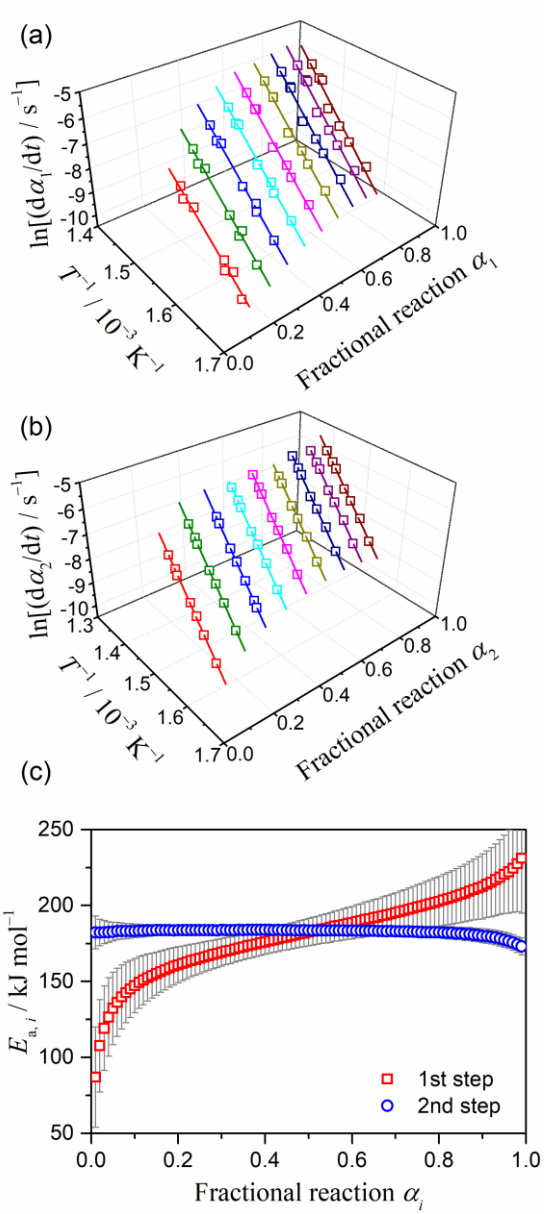

Figure S9. Isoconversional kinetic analysis performed on the mathematically separated kinetics curves: (a) Friedman plots for the first reaction step, (b) Friedman plots for the first reaction step, and (c) $E_{a,i}$ values at different α_i.

For the second reaction step characterized by a constant E_a value, the experimental master plot in differential form was drawn according to eq. (9). In Figure S10 are reported the $(d\alpha_2/d\theta_2)$ values at different α_2 values for the second reaction step (i = 2). The $(d\alpha_2/d\theta_2)$ versus α_2 plot is characterized by the presence of a maximum at $\alpha_2 = 0.47$. For fitting the experimental master plot to $f(\alpha)$ according to eq. (9), an empirical kinetic model function known as the Šesták–Berggren model (eq. (7)), SB(m, n, p), was used, because of its high flexibility to fit various types of reactions controlled by different physico-geometries and those deviated cases. Because of the characteristic shape of the experimental master plot, which displays a

maximum midway through the reaction, the fitting using a nucleation-growth type kinetic model (eq. (11)), JMA(m), was also examined. The experimental master plot was fit by SB(−0.33 ± 0.02, 1.11 ± 0.01, 0.92 ± 0.02) and JMA(2.52 ± 0.01), accompanied by A_2 values of (1.39 ± 0.01) × 10^{12} s^{-1} and (5.70 ± 0.01) × 10^{11} s^{-1}, respectively, indicating high statistical significance (r^2 > 0.999) in both the fittings.

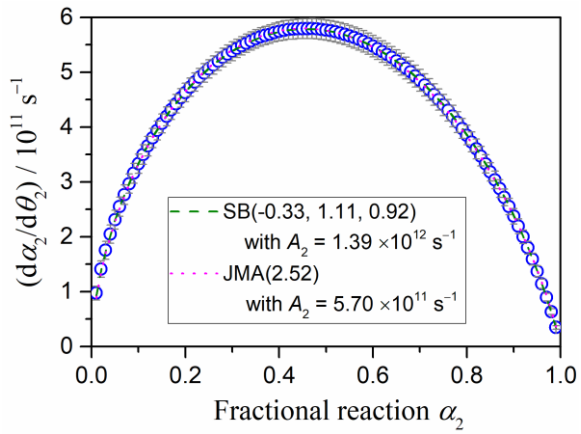

Figure S10. Experimental master plot of ($d\alpha_2/d\theta_2$) versus α_2 for the second reaction step (i =2), drawn on the basis of the relevant mathematically separated kinetic curves.

S5. Thermal behavior of $Ca(OH)_2$ in CO_2 atmosphere

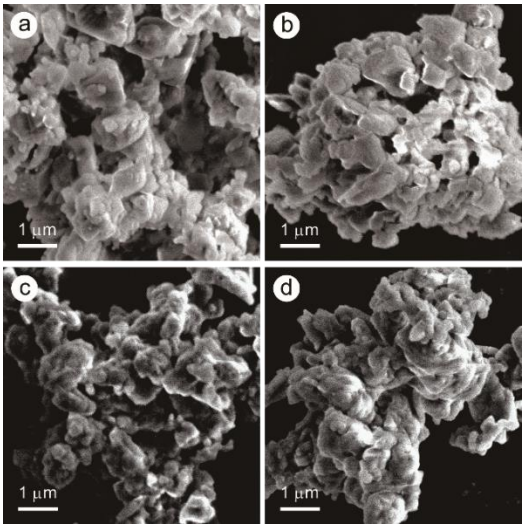

Figure S11. Typical SEM images of the sample particles that had undergone partial reaction with CO_2 as a consequence of being heated linearly to different final temperatures at β = 5 K min^{-1} in a stream of flowing N_2–CO_2 mixed gas (CO_2 concentration: 15%; flow rate: 300 cm^3 min^{-1}): (a) T = 573 K (α = 0.00), (b) T = 673 K (α = 0.12), (c) T = 773 K (α = 0.74), and (d) T = 898 K (α = 1.00).

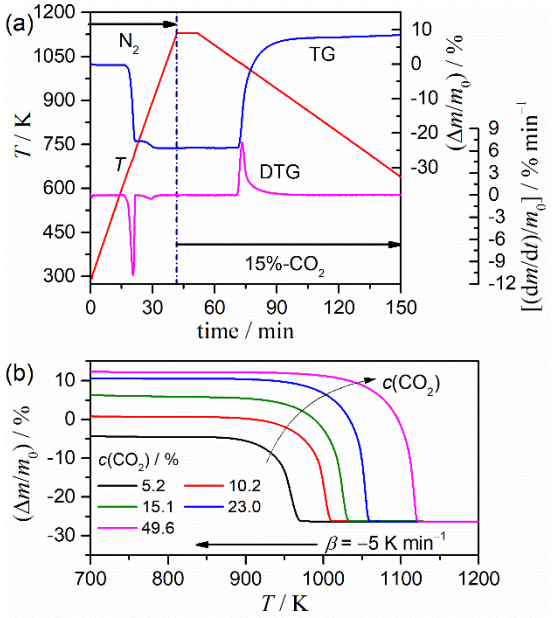

Figure S12. TG curves for the carbonation of CaO as produced by the thermal decomposition of $Ca(OH)_2$ (m_0 = 3.00 ± 0.05 mg) upon cooling at β = −5 K min^{-1} in a stream of N_2–CO_2 mixed gas (flow rate: 300 cm^3 min^{-1}): (a) typical TG–DTG curves recorded during a reaction performed in a stream of N_2–CO_2 mixed gas (CO_2 concentration: 15%) and (b) TG curves recorded during the reactions performed in a stream of N_2–CO_2 mixed gases of different CO_2 concentrations.

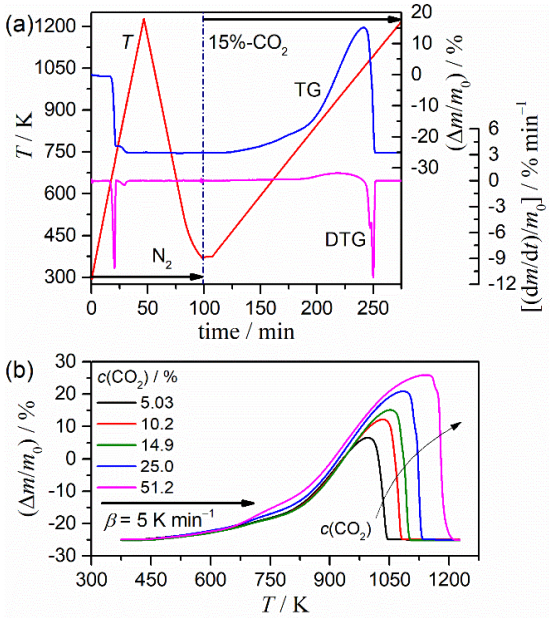

Figure S13. TG curves for the carbonation of CaO as produced by the thermal decomposition of $Ca(OH)_2$ (m_0 = 3.00 ± 0.05 mg) upon heating at β = 5 K min^{-1} in a stream of N_2–CO_2 mixed gas (300 cm^3 min^{-1}): (a) typical TG–DTG curves recorded during a reaction performed in a stream of N_2–CO_2 mixed gas (CO_2 concentration: 15%) and (b) TG curves recorded during the reactions performed in a stream of N_2–CO_2 mixed gases of different CO_2 concentrations.

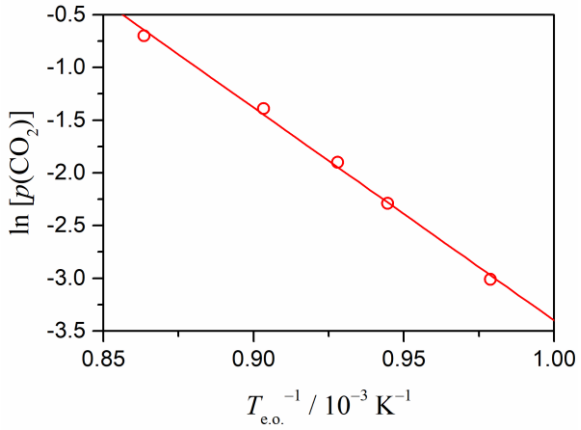

Figure S14. The van't Hoff plot for the $CaCO_3(s) \rightleftarrows CaO(s) + CO_2(g)$ equilibrium reaction at different $p(CO_2)$ examined using the extrapolated onset temperature of the thermal decomposition of $CaCO_3$ produced by the reaction of $Ca(OH)_2$ and CO_2.

S6. Kinetics of the thermally induced carbonation of $Ca(OH)_2$

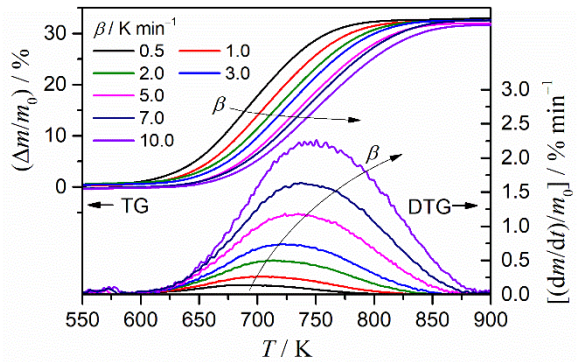

Figure S15. TG–DTG curves for the reaction of $Ca(OH)_2$ (m_0 = 3.00 ± 0.05 mg) with CO_2 in a stream of N_2–CO_2 mixed gas (CO_2 concentration: 15%; flow rate: 300 cm^3 min^{-1}) recorded under linear nonisothermal conditions at different β.

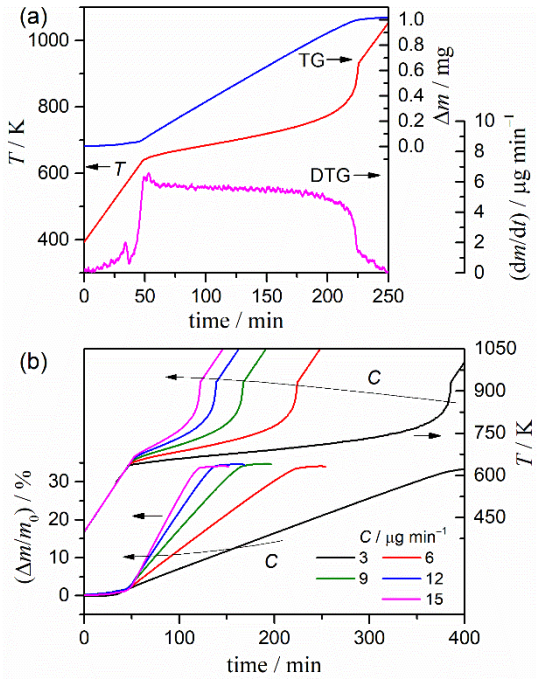

Figure S16. TG–DTG curves for the reaction of $Ca(OH)_2$ (m_0 = 3.00 ± 0.05 mg) with CO_2 in a stream of N_2–CO_2 mixed gas (CO_2 concentration: 15%; flow rate: 300 cm^3 min^{-1}) recorded under CRTA conditions: (a) typical CRTA curves recorded at C = 6 μg min^{-1} and (b) at different C.

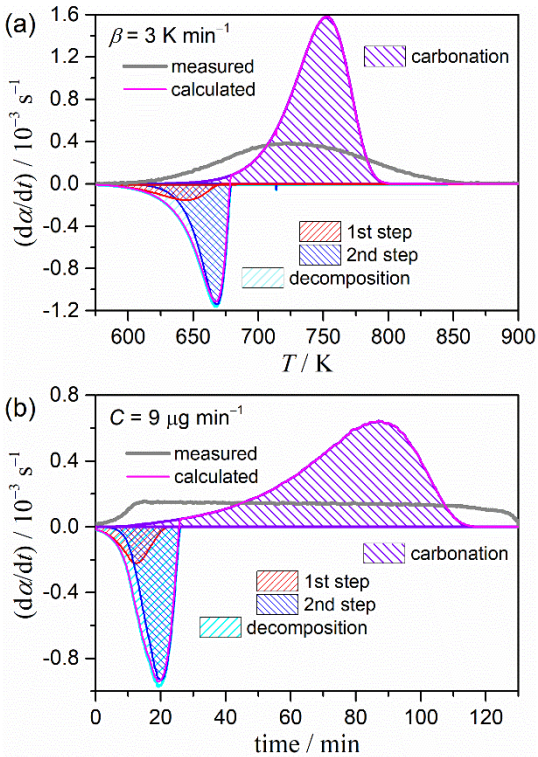

Figure S17. Typical initial settings of a KDA performed on the reaction of $Ca(OH)_2$ with CO_2 in a stream of N_2–CO_2 mixed gas (CO_2 concentration: 15%; flow rate: 300 cm^3 min^{-1}) for the kinetic data recorded under (a) linear nonisothermal conditions at β = 3 K min^{-1} and (b) CRTA conditions at C = 9 μg min^{-1}.